André Weber*

Impedance analysis of porous electrode structures in batteries and fuel cells

Impedanzanalyse poröser Elektrodenstrukturen in Batterien und Brennstoffzellen

https://doi.org/10.1515/teme-2020-0084
Received November 12, 2020; accepted December 5, 2020

Abstract: Today technical electrodes in batteries and fuel cells rely on complex multiphase microstructures that facilitate electronic, ionic and, in case of fuel cells, diffusive gas transport to the active reaction sites distributed in the electrode volume. The impedance of such electrodes can be described by the well-established transmission line model (TLM) approach. In a TLM, transport, charge transfer phenomena and capacitive effects are coupled considering microstructural features of the electrode. Its application for impedance data analysis of technical cells is challenging as the TLM impedance extends over a wide frequency range and quite often a strong overlapping with other contributions takes place.

In this paper the application of the distribution of relaxation times (DRT) to the analysis of technical electrodes in batteries and fuel cells is elucidated. Different examples how to apply the DRT to analyze impedance spectra of solid oxide-, polymer electrolyte- and lithium ion-cells will be discussed. It will be shown that the TLM is usually represented by multiple peaks in the DRT, which might be strongly affected if contributions of different electrode layers overlap in the spectra. Related error sources and countermeasures are illustrated. Approaches how the DRT can be applied for the analysis of measured spectra and how it is able to support CNLS-fitting are presented.

Keywords: Electrochemical impedance spectroscopy, distribution of relaxation times, transmission line model, lithium ion battery, fuel cell, LiB, SOFC, SOEC, SOC, PEMFC.

Zusammenfassung: Technische Elektroden in Batterien und Brennstoffzellen beruhen auf komplexen mehrphasigen Mikrostrukturen, die elektronischen, ionischen und Gasphasen-Transport zu den im Elektrodenvolumen verteilten aktiven Reaktionszonen realisieren. Die Impedanz solcher Elektroden kann mit Kettenleitermodellen beschrieben werden. In diesen werden Transportprozesse, Ladungstransferphänomene und kapazitive Effekte unter Berücksichtigung mikrostruktureller Eigenschaften der Elektrode gekoppelt. Ihre Anwendung in der Impedanzanalyse technischer Zellen ist anspruchsvoll, da sich die Kettenleiterimpedanzen über einen weiten Frequenzbereich erstrecken und häufig starke Überlappungen der Impedanzen unterschiedlicher Prozesse in der Zelle vorliegen.

In diesem Beitrag wird die Anwendung der Verteilungsfunktion der Relaxationszeiten (DRT: Distribution of Relaxation Times) in der Analyse technischer Elektroden in Batterien und Brennstoffzellen beleuchtet. Es werden verschiedene Beispiele für die Einsatz der DRT zur Entfaltung der Impedanzspektren von Festoxid-, Polymerelektrolyt- und Lithium-Ionen-Zellen diskutiert. Die Beispiele zeigen, dass die DRT der Impedanz poröser Elektrodenstrukturen häufig mehrere Peaks aufweist, die durch Überlagerung der Beiträge verschiedener Elektrodenschichten beeinflusst werden. Daraus resultierende Fehlerquellen, mögliche Gegenmaßnahmen und Ansätze, wie die DRT für die Analyse gemessener Spektren und den CNLS-Fit von Impedanzdaten eingesetzt werden kann, werden vorgestellt.

Schlagwörter: elektrochemische Impedanzspektroskopie, Verteilungsfunktion der Relaxationszeiten, Kettenleitermodell, Lithium-Ionen Batterie, Brennstoffzelle, LiB, SOFC, SOEC, SOC, PEMFC.

1 Introduction

Electrochemical devices as lithium ion batteries, fuel cells and electrolyzers enable a reversible electrochemical energy conversion between electrical energy and chemical energy stored either in the active materials of the battery's electrodes or a fuel, mostly hydrogen. In such devices, high conversion rates per unit cell area are mandatory to meet size, weight and last but not least cost requirements of the system. To achieve a high area specific conversion rate, a large number of active reaction sites per unit area is required. This can be achieved by extending

***Corresponding author: André Weber,** Karlsruhe Institute of Technology (KIT), Institute of Applied Materials (IAM-WET), Adenauerring 20b, 76131 Karlsruhe, Germany, e-mail: andre.weber@kit.edu

the electrochemical reactions at the 2-dimensional electrode / electrolyte interface into the 3-dimensional volume of the electrodes. Such approach is not at all new, already in the beginning of electrochemistry and fuel cells, more than 170 years ago, it was observed that a "notable surface of action" can be achieved by a "spongy platina" electrode [1]. The porous electrode structure enhances the area specific conversion rate as active reaction sites are extended into the electrode volume and are no longer restricted to a planar interface. This approach is state of the art in electrochemistry since many decades. Today nearly all electrochemical devices for energy storage and conversion rely on porous, multiphase electrodes and there is only a very limited number of devices, as for example thin film batteries, where the charge transfer reaction is restricted to a planar interface between electrode and electrolyte.

Even though a qualitative understanding of the advantages of porous electrode structures was available right from the start, the quantitative electrochemical and microstructural characterization and subsequent modelling is still a hot topic in battery and fuel cell research. There are numerous publications related to the development and characterization of porous electrodes and full cells exhibiting two of them respectively.

A common method for the electrochemical characterization of batteries and fuel cells is impedance spectroscopy. Theoretical background and practical information can be found in a number of handbooks [2, 3, 4, 5]. Within the impedance measurement the electrochemical cell is considered to be a LTI system, even if electrochemical systems are usually neither linear nor time invariant. Thus the electrochemical impedance has to be measured via a rather small sinusoidal perturbation in the range of a few mV; aiming at a stimulation of the cell in a linear or at least linearizable range. Any additional impact of the perturbation signal on the cell's temperature or state of charge (SoC) should be carefully avoided. The variation of the perturbation frequency over several decades (mHz to MHz) provides the electrochemical impedance spectrum. For the subsequent analysis of a measured spectrum any kind of error source as improper wiring or unsuitable settings [6] has to be avoided. The validity testing of measured spectra is indispensable. Algorithms based on the Kramers-Kronig relation enable a detection of errors due to nonlinearities, time variance or external noise in the spectra [7, 8, 9].

Electrochemical impedance spectroscopy (EIS) is often applied to determine or compare the performance of cells and electrodes. Such performance evaluation is straightforward and does not require any complex impedance data analysis. If the different physicochemical processes in a cell are of interest and the development and parameterization of an electrochemical model is in focus, impedance data analysis becomes mandatory. In a first step, a deconvolution of the spectra by methods as the distribution of relaxation times (DRT) [10] is useful. The DRT enhances the resolution in the frequency domain and is able to resolve processes invisible in common impedance representation as Nyquist or Bode plots [11, 12]. Based on their relaxation frequencies and operating parameter dependencies, the peaks in the DRT can be assigned to physicochemical processes in the cell [13, 14] and thus provides fundamental information for electrochemical modelling.

In case of technical cells with porous electrodes appropriate electrochemical models, representing the coupling of transport processes and electrochemical reactions, are required. There are different types of complex electrochemical models for porous electrodes. Homogenized approaches based on equivalent circuit theory [15] or a set of differential equations [16, 17] date back to the 60th. The Newman model for lithium ion battery electrodes is a prominent example [18, 19], which was later on extended in various ways [20, 21]. In case of fuel cells, elementary kinetic models of reaction and transport processes were employed [22, 23]. With increasing computing power and the availability of 3D electrode reconstructions by FIB-SEM [24, 25] and X-ray tomography [26, 27] space resolved models of porous electrodes became popular [28, 29, 30]. Such homogenized as well as space resolved approaches have also been used to model impedance spectra of electrodes and cells [21, 31, 32, 33, 34]. As these models cover complex nonlinearities related to charge transfer and diffusive processes with dozens of material and interfacial parameters they are mostly too complex for a direct quantitative correlation to measured impedance spectra.

In case of impedance spectroscopy the fundamental requirements – linearity (or linearizability in the operating point), time invariance and causality – simplify the modelling. Linear and time invariant (LTI) modelling approaches as equivalent circuit models (ECM), based on electrical standard components as resistors and capacitors, can be applied. Thus computing time as well as number of model parameters can be drastically reduced. The model parameters can "easily" be determined by a complex nonlinear least square (CLNS) fit [35] using appropriate tools [36, 37], which are nowadays part of most impedance analyzer software packages.

ECMs differ with respect to the correlations between equivalent circuit elements and physicochemical pro-

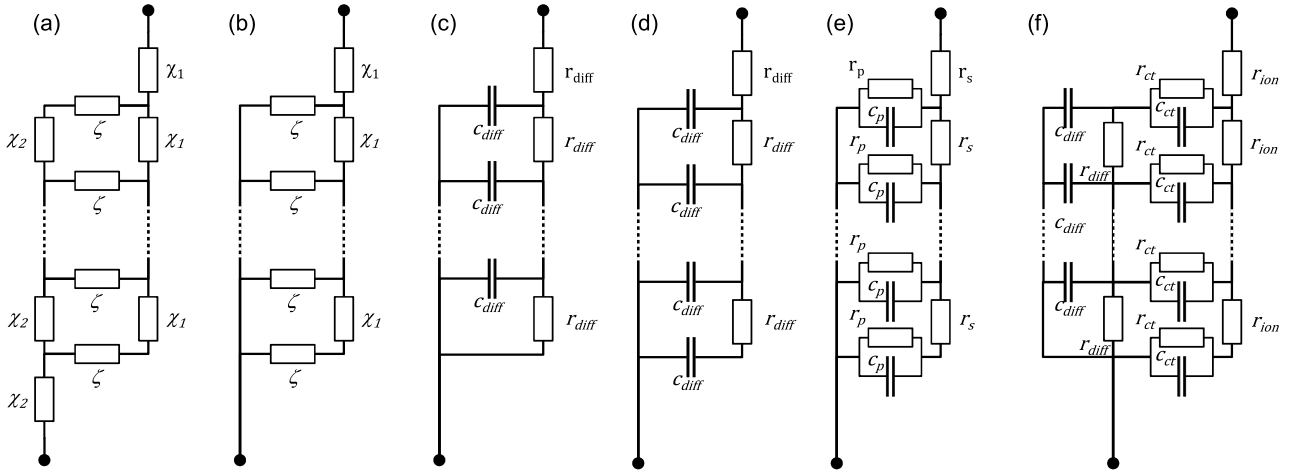

Figure 1: Transmission line equivalent circuits for different types of electrodes (a) general 2 channel transmission line model with χ_1 and χ_2 representing ionic and electronic resistances coupled by the charge transfer impedance ζ, (b) simplified single channel approach commonly applied in case of negligible electronic resistivity, (c) finite length and (d) finite space Warburg impedance, (e) Gerischer impedance and (f) three channel transmission line model coupling ionic and gas phase transport via a charge transfer reaction.

cesses. In black box approaches the ECM just reproduces the system dynamics. It is mostly based on a series connection of a sufficient number of RC-elements (parallel connection of a resistance R and a capacitance C) whereby the equivalent circuit elements do not have any physicochemical meaning. Such models are applied in battery-module and BMS-development [38, 39, 40]. Despite of their non-physical character they enable reliable simulations in the frequency and time domain [41]. In case of physicochemically meaningful ECMs, quite often electrode processes observed in the spectrum are represented by R-CPE elements (parallel connection of a resistance R and a constant phase element CPE) [13, 42, 43, 44]. With this simplified approach the overall impedance of each electrode process becomes available but any quantitative correlation with material properties or microstructural features of the porous electrode is impossible. For a more detailed modelling appropriate equivalent circuit elements as Warburg [45, 46] or Gerischer impedances [47] are required. Such equivalent circuit elements are all based on transmission line models (TLM) – physicochemically meaningful ECMs that represent the coupling of transport, reaction and/or storage in the volume of a porous electrode [48].

In this paper examples of DRT-analysis and transmission line modeling of porous electrodes in solid oxide cells, polymer electrolyte membrane fuel cells and lithium ion batteries are compared. Requirements concerning impedance spectroscopy, data quality and DRT-analysis are discussed and different approaches for model parameterization are presented.

2 Theoretical background

The general transmission line equivalent circuit sketched in Fig. 1 (a) represents the impedance of a porous electrode with a thickness L.

It exhibits the TLM-impedance Z_{TLM} according to eqn. (1):

$$Z_{\mathrm{TLM}}(\omega) = \frac{\chi_1\chi_2}{\chi_1+\chi_2}\cdot\left(L+\frac{2\cdot\kappa}{\sinh(L/\kappa)}\right)+\kappa\cdot\frac{\chi_1^2+\chi_2^2}{\chi_1+\chi_2}\cdot\coth\left(\frac{L}{\kappa}\right) \tag{1}$$

The series elements χ_1 and χ_2 account for the ionic, electronic or diffusive transport pathways in the porous electrode. Regardless of the type of transport process i, (index i: *ion*, *electron*, *diff*), they are mostly represented by an incremental ohmic resistance per unit length r_i (Ω/m), which is suitable because of the linearization in impedance spectroscopy. In case of capacitive effects along the transport path an RC or RCPE-element can be used instead. For ionic or electronic transport in an electrical field r_i is depending on the bulk conductivity σ_i and the structural factor ψ_i, the ratio between the volume fraction ε_i and the tortuosity τ_i of the corresponding phase:

$$\chi_i = r_i = \frac{1}{\sigma_{i,eff}}\cdot\frac{1}{A_{cell}} = \frac{1}{\sigma_i}\cdot\frac{1}{\psi_i}\cdot\frac{1}{A_{cell}} \tag{2}$$

A diffusive transport of neutral gaseous species (gas diffusion in the pores of the electrode) respectively ions in a mixed ionic-electronic conductor (MIEC) with a dominant electronic conduction (as oxygen ion diffusion in MIEC cathodes of solid oxide fuel cells (SOFC) or Li-diffusion in intercalation electrode materials of lithium ion

batteries) can be described by a diffusion resistance r_{diff} (Ω/m) that is depending on the effective diffusion coefficient $D_{i,eff} = \psi_i D_i$ of the diffusing species and its concentration c_i (mol/m^3). In case of gases the partial pressure $p_i = RT \cdot c_i$ of the diffusing gas species is commonly used. z_i is the valency of the diffusing ion or, in case of neutral species as gases, the number of transferred electrons in the related electrochemical reaction respectively. The resistive character of such diffusive process is related to the coupling of the concentration gradient required for diffusion according to Fick's law and its impact on the electrode potential via the Nernst equation.

$$\chi_i = r_{diff} = \frac{RT}{(z_i F)^2} \cdot \frac{1}{D_{i,eff}} \cdot \frac{1}{c_i} \cdot \frac{1}{A_{cell}} = \left(\frac{RT}{z_i F}\right)^2 \cdot \frac{1}{D_{i,eff}} \cdot \frac{1}{p_i} \cdot \frac{1}{A_{cell}} \tag{3}$$

The localized processes within the porous electrode volume as charge transfer reactions and/or capacitive storage are represented by the shunt branch impedance ζ given in Ω·m. The ratio κ of shunt branch impedance ζ and the sum of the series elements χ_1 and χ_2 provides information about the local distribution of transport processes, reaction and storage in the electrode volume.

$$\kappa = \sqrt{\frac{\zeta}{\chi_1 + \chi_2}} \tag{4}$$

In case of large κ-values the transport is sufficiently fast and homogeneous conditions are achieved. The same holds for $\chi_1 = \chi_2$, as long as both transport pathways exhibit a similar resistance there will be no preferred section where reactions will take place. If $\chi_1 \gg \chi_2$, a common situation for most electrodes exhibiting an electronic conductivity that is orders of magnitude above their ionic conductivity, it is suitable to neglect the resistive contribution of χ_2 resulting in the single channel TLM (Fig. 1 (b)) with the simplified impedance expression:

$$Z_{TLMsc}(\omega) = \kappa \cdot \chi_1 \cdot \coth\left(\frac{L}{\kappa}\right) = \sqrt{\zeta \cdot \chi_1} \cdot \coth\sqrt{\frac{\chi_1 \cdot L^2}{\zeta}} \tag{5}$$

Under this condition ($\chi_2 = 0$) the ratio κ corresponds to the penetration depth $\lambda = \sqrt{\zeta / r_1}$ providing information about the active thickness of the electrode. Within the distance λ from the electrolyte/electrode-interface into the electrode volume 67 % of the electrochemical conversion takes place.

There is a large number of dedicated transmission line models available describing the impedance for a particular coupling of transport, charge transfer and/or capacitive effects in battery and fuel cell electrodes. The Finite Space Warburg impedance Z_{FSW} and Finite Length Warburg impedance Z_{FLW} consider a coupling of diffusion and capacitive storage in an electrode. They correspond to the equivalent circuits in Fig. 1 (c) and (d) with short circuited and open end respectively. The related time constant $\tau_{diff} = r_{diff} \cdot c_{diff} \cdot L^2$ considers the overall resistance $r_{diff} \cdot L$ and capacitance $c_{diff} \cdot L$ of the layer:

$$Z_{FSW}(\omega) = \kappa \cdot r_{diff} \cdot \coth\left(\frac{L}{\kappa}\right) = r_{diff} \cdot L \cdot \frac{\coth\sqrt{j\omega\tau_{diff}}}{\sqrt{j\omega\tau_{diff}}} \tag{6}$$

$$Z_{FLW}(\omega) = \kappa \cdot r_{diff} \cdot \tanh\left(\frac{L}{\kappa}\right) = r_{diff} \cdot L \cdot \frac{\tanh\sqrt{j\omega\tau_{diff}}}{\sqrt{j\omega\tau_{diff}}} \tag{7}$$

Whereas Z_{FSW} describes the diffusion of species from a limited reactant source represented by c_{diff} as the lithium stored in the active material of a battery, Z_{FLW} is representing the diffusion of species from an infinite reactant source (as the gas channel in a fuel cell) through a porous layer. Here the capacitive behavior of the pore volume as well as adsorption of gaseous species at surfaces is represented by c_{diff}. To account for non-uniform electrode parameters quite often a generalized form (Z_{GFSW}/Z_{GFLW}) is applied where $\sqrt{j\omega\tau_{diff}}$ is replaced by $(j\omega\tau_{diff})^n$ with physically meaningful exponents of $n \leq 0.5$.

The Gerischer impedance $Z_{Gerischer}$ originally dates back to studies of coupled chemical and electrochemical reactions [47], different applications are summarized in [49]. It describes an electrode with an infinite thickness ($L \to \infty$) that is represented by an equivalent circuit according to Fig. 1 (e). Its impedance is given by eqn. (8) wherein the coth-term becomes 1 for $L/\lambda \gg 1$. The Gerischer element is often applied for MIEC electrodes in SOFC [50]. In this approach only oxygen surface exchange and oxygen ion diffusion in the MIEC bulk is considered whereas electronic conduction and gas diffusion are neglected [51].

$$Z_{Gerischer}(\omega) = \frac{R_{chem}}{\sqrt{1 + j\omega\tau_{chem}}}$$
$$\text{with } R_{chem} = \frac{RT}{2F^2} \cdot \frac{1}{A_{cell}} \cdot \sqrt{\frac{\tau \cdot \gamma^2}{(1-\varepsilon) \cdot D_\delta \cdot a \cdot c_{mc}^2 \cdot k^\delta}},$$
$$t_{chem} = \frac{c_O \cdot (1-\epsilon)}{a \cdot c_{mc} \cdot k^\delta} \tag{8}$$

Both processes are affected by material (oxygen ion diffusion coefficient D^δ, surface exchange coefficient k^δ, density of oxygen lattice sites c_{mc}, oxygen ion concentration c_O, thermodynamic factor γ) and microstructural properties (porosity ε, MIEC tortuosity τ, surface area density a of the porous MIEC electrode. Considering the equivalent circuit in Fig. 1 (e) $R_{chem} = r_s \cdot r_p$ and $\tau_{chem} = r_p \cdot c_p$.

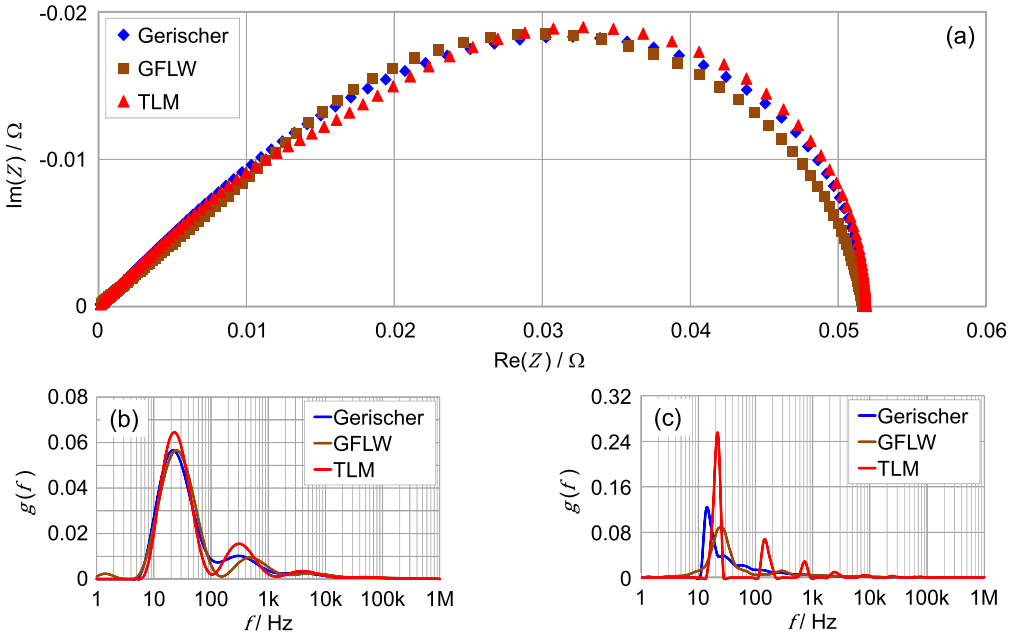

Figure 2: Nyquist plot of Gerischer, GFLW and single channel TLM impedance with parameter sets resulting in rather similar spectra and related DRTs. In the DRT plots different regularization parameters of 10^{-3} (left) and 10^{-14} (right) were applied.

In Fig. 2 (a) impedance spectra of Gerischer, GFLW and single channel TLM according to the equations given above are displayed in a Nyquist plot. The parameters were selected in a way that quite similar spectra are obtained. It should be noted that these parameters were all kept in physicochemically meaningful ranges observed for different kinds of SOFC electrodes tested under technically meaningful operating conditions. Considering noise and minor errors unavoidable in impedance measurements, the selection of an appropriate TLM based on the measured spectrum only is hardly possible.

Below the DRTs of the spectra are displayed. Instead of $\gamma(\tau)$ a corresponding function $g(f)$ is commonly displayed, which is logarithmically weighted in a way that the area under each peak corresponds to the resistance of the related process. This approach enables a quantitative visualization of the polarization resistances and a direct correlation to their relaxation frequencies. Despite of the fact that only one electrode process is present in each spectrum, the DRTs contain, next to a dominant peak at the main relaxation frequency, a number of side peaks at different frequencies. This behavior is related to the numerical calculation of the DRT $\gamma(\tau)$.

$$Z(\omega) = R_0 + Z_{pol}(\omega) = R_0 + \int_0^\infty \frac{\gamma(\tau)}{1 + j\omega\tau} \mathrm{d}\tau \qquad (9)$$

The solution of the equation for $\gamma(\tau)$ is an ill posed problem that requires special methods to avoid false peaks and oscillations. In this paper all DRTs were calculated using a Tikhonov regularization algorithm according to [52], which is based on stabilizing a minimization problem by introducing a regularization operator that is weighted with a regularization parameter λ. In case of distributed elements as in a TLM, the highly asymmetric spectrum has to be emulated by a discrete number of RC-elements with relaxation frequencies dispersed over several orders of magnitude. Thus, there will always be a strong impact of the selected regularization parameter on the shape of the DRT. In Fig. 2 (b) a regularization parameter $\lambda = 10^{-3}$ is applied. This value is in a suitable λ range for the analysis of experimental data, smoothing out noise and minor errors and suppressing artificial peaks. The DRTs of the different TLMs show some differences with respect to the 2nd peak at 100 Hz to 1 kHz. If a much smaller regularization parameter is applied (Fig. 2 (c)), which is only suitable for noise and error free synthetic spectra and would result in severe deviations for experimental data, a different shape much closer to the analytical DRTs of the different elements [12] is obtained. It is obvious, that number, shape and positions of the peaks are affected by the selection of the regularization parameter. The existence of these side peaks and their dependency on calculation procedures and parameters complicates the DRT-analysis of porous electrodes. The straightforward approach to attribute each peak in the DRT to a single polarization process in the cell and to quantify its resistance contribution directly from the DRT can

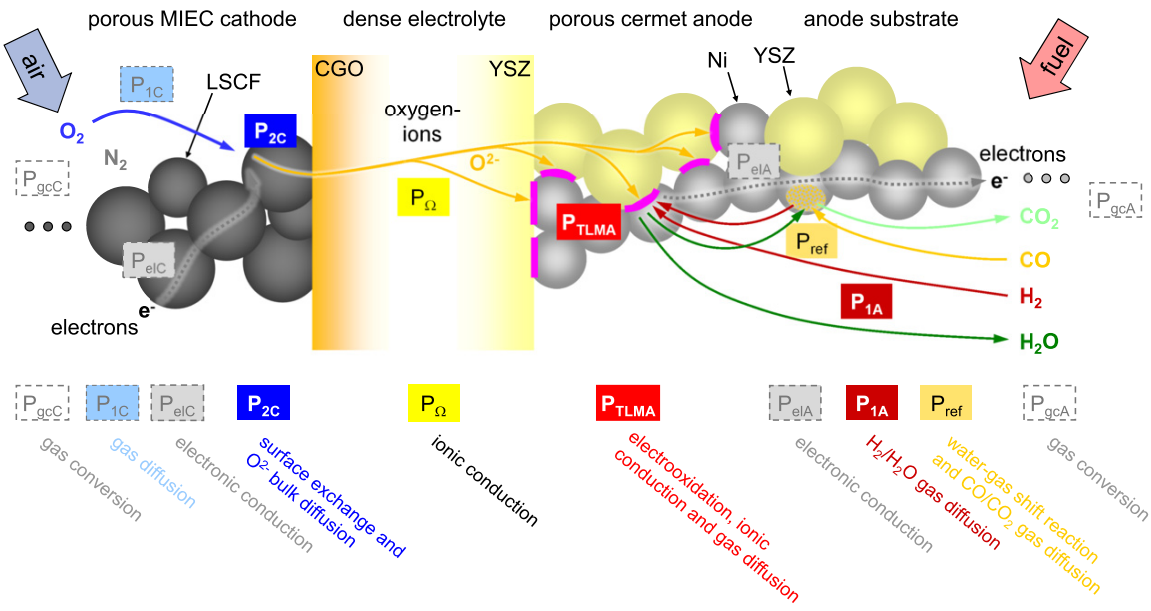

Figure 3: Polarization processes in the porous electrodes of an anode supported SOFC. Transport and electrochemical reactions in the MIEC cathode and the cermet anode (ceramic-metal compound of oxide ion conducting ceramic electrolyte and electronically conducting nickel) can be described by appropriate TLMs, a Gerischer impedance (P_{2C}) and a transmission line model (P_{TLMA}) respectively. Due to limited ionic transport in the MIEC and the electrolyte, the thickness of the electrochemically active regions is in the range of a few µm only. In the remaining parts of the porous electrodes and supports electronic conduction, gas diffusion and catalytic conversion of the fuel has to be considered.

lead to significant errors. A simple straightforward DRT-analysis of experimental data does not provide direct access to a physicochemical meaningful TLM as different processes like the gas diffusion through a porous layer or the oxygen reduction reaction in a MIEC cathode can provide quite similar spectra and DRTs. In the following some examples for the analysis of porous fuel cell and battery electrodes by transmission line models are discussed and critical aspects concerning their parameterization are shown.

3 Application to porous electrodes in fuel cells and batteries

Transmission line models can be applied to evaluate and predict the behavior of porous electrodes in different ways. The complex nonlinear least squares (CNLS-) fitting of a physicochemically meaningful ECM to measured impedance spectra can be used for the quantification of the individual losses related to the different polarization processes occurring in the investigated cell. The gathered information enables an assessment of the cell, provides a correlation to material and microstructural parameters of its electrodes and reveals approaches for its optimization. For this approach (i) a physicochemically meaningful ECM has to be developed, (ii) starting parameters for the CNLS-fit have to be determined and (iii) the CNLS-fit has to be performed considering appropriate parameter ranges. Considering technical cells this is challenging as the electrodes have been optimized. Mostly there is not a single rate limiting step but different polarization processes with resistance contributions in a similar range, which might strongly overlap in the impedance spectrum. Thus powerful impedance analysis tools as the distribution of relaxation times combined with appropriate variations of operating conditions are mandatory to resolve the individual processes.

3.1 Solid oxide fuel cells

One example is the impedance analysis of solid oxide fuel cells [13] whose impedance is affected by gas diffusion and conversion in porous supports and electrodes as well as electrochemical reactions coupled with ionic and gas phase transport in the electrode volumes close to the electrode / solid electrolyte interfaces (Fig. 3) [13, 53]. Thus a number of serial connected transmission line models are required for a physicochemically meaningful ECM of the cell.

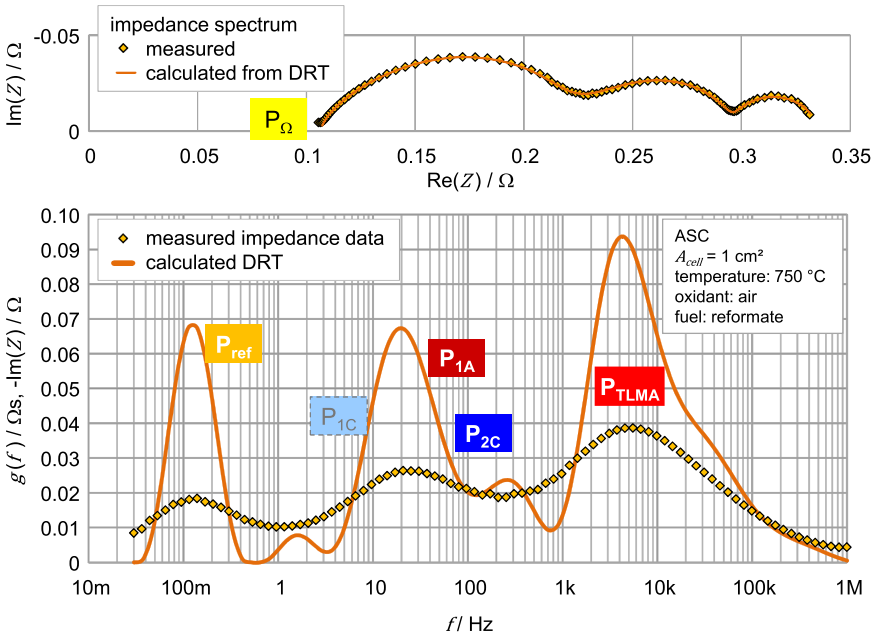

Figure 4: Impedance spectrum and DRT of an anode supported solid oxide fuel cell operated with a reformate fuel.

Fig. 4 shows a typical impedance spectrum of an anode supported cell (ASC) in the Nyquist plot (top) and the imaginary part of the impedance vs. frequency as well as the DRT (bottom). At first glance it is obvious that the DRT provides additional information as some of the peaks in the DRT are not observable in the impedance spectrum.

To set up a physicochemically meaningful model the observable peaks have to be attributed to related polarization processes. By means of extensive operating parameter variations characteristic dependencies of the individual peaks can be obtained [13]. Specific operating conditions, which minimize or prevent certain polarization processes, can simplify the analysis. Gas conversion (P_{gc}) can be minimized by a high stoichiometry and small active cell area, humidified hydrogen instead of complex reformates eliminates the low frequency process (P_{ref}) related to the coupling of water-gas shift reaction and CO/CO_2 gas diffusion [53] whereas pure oxygen instead of compressed air suppresses gas diffusion at the cathode (P_{1C}). Some polarization processes as the diffusive transport of fuel gas and the related reaction product (P_{1A}) cannot be prevented but minimized or shifted with respect to the related relaxation frequency. A CO/CO_2-mixture instead of hydrogen/steam exhibits a much lower binary gas diffusion coefficient. Accordingly the gas diffusion process is shifted to much lower relaxation frequencies and the cathode process can be uncovered [54]. The concept of a DRT-based deconvolution of impedance spectra is elucidated in Fig. 5 that shows the DRTs of Gerischer element and Warburg element (GFLW) representing P_{2C} and P_{1A} respectively. In measured impedance spectra only the sum GFLW + Gerischer is accessible. In case of H_2/H_2O-fuel and a regularization parameter of 10^{-3} – even in case of ideal data without any noise and errors – the regularization in the DRT merges Gerischer and GFLW into one peak (Fig. 5 (a)). Thus no deconvolution is possible. If the regularization parameter is reduced to 10^{-8} the two processes could be deconvolved in the DRT, but only if ideal impedance data would be available (Fig. 5 (b)). In case of small errors (randomly distributed error, |error| < 1.6 mΩ) or a limited resolution of the measuring device, a low regularization parameter results in inconsistent DRT-peaks that rule out any conclusion about the underlying polarization processes (Fig. 5 (c)). It should be stated that even with the use of the DRT the deconvolution of TLM polarization processes with narrow relaxation times is challenging. Especially in case of new, unknown electrochemical cells possible error sources leading to misinterpretations of the spectra have to be considered. By far a better approach is to shift overlapping processes by changing testing conditions. In case of a CO/CO_2-mixture as the fuel (Fig. 5 (d)) a reliable deconvolution of the two processes becomes possible.

However, in case of TLM-impedances a direct quantitative analysis of the DRT should be avoided as contributions of the 2nd and 3rd peak of the GFLW-element are attributed to the main peak of the Gerischer element, resulting in an overestimated cathode polarization resistance. The subsequent CNLS-fit of the impedance spectrum using

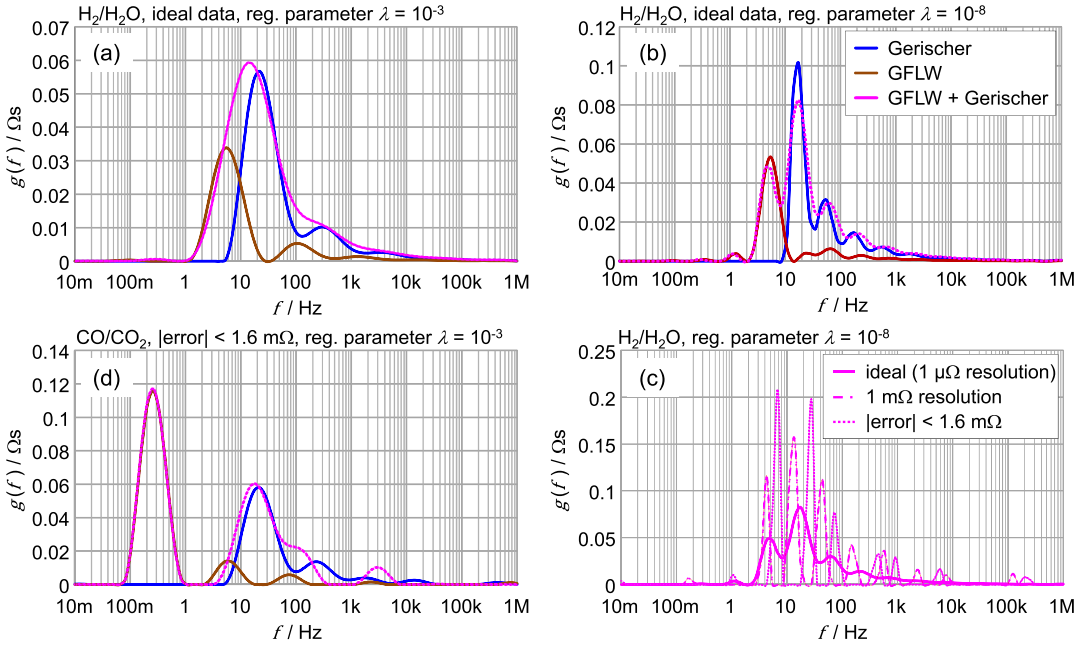

Figure 5: DRTs of the Gerischer element (P_{2C}) and the GFLW (P_{1A}) and the resulting sum as existent in the impedance spectrum of an anode supported SOFCs for ideal (top) and noisy impedance data (bottom). The DRTs were calculated with a regularization parameter of 10^{-3} (left) suitable for experimental data and 10^{-8} (right) leading to artificial peaks in the DRT of noisy impedance data.

an appropriate ECM and starting values provided by the DRT enables precise quantitative result because the contributions of the side peaks at higher frequencies are correctly assigned in the fit.

The obtained results can be used to determine characteristic parameters of the electrodes. For the diffusion of reactants (index: *rt*) and reaction products (index: *rp*) in the anode substrate the diffusion resistance R_{diff} obtained from the CNLS-fit is correlated to parameters of the fuel gas and the pore structure by an adapted form of eqn. (3):

$$R_{diff} = r_{diff} \cdot L = \left(\frac{RT}{z_i F}\right)^2 \cdot \frac{L}{\psi_{pore}} \cdot \frac{1}{A_{cell}} \cdot \left(\frac{1}{D_{rt} \cdot p_{rt}} + \frac{1}{D_{rp} \cdot p_{rp}}\right) \tag{10}$$

Using eqn. (10), ψ_{pore} respectively the ratio L/ψ_{pore} can be determined and the diffusion resistance R_{diff} for any desired fuel gas mixture can be calculated. The diffusion coefficients, which consider the impact of Knudsen diffusion and thus require additional information about the pore size distribution, have to be calculated [55].

With the Gerischer element fundamental material parameters as the oxygen ion diffusion coefficient D^{δ} and the surface exchange coefficient k^{δ} of MIEC-materials can be extracted from the CNLS-fit [56]. The microstructural parameters in eqn. (8), which can be obtained by means of tomography, are mandatory for a precise quantification [51]. It should also be noted that this approach is limited to MIEC-electrodes that fulfill the preconditions for applying a Gerischer element, which is not always the case [57].

Considering the parameterization of TLMs as used for the coupling of charge transfer reaction and ionic conduction in SOFC anodes [58] or PEMFC cathodes [59] an ambiguity of the TLM has to be considered. In eqn. (5) the coth-term becomes approximately one if the electrode thickness is exceeding the penetration depth by far. In this case the impedance is solely determined by $\zeta \cdot \chi_1$. A CNLS-fit of eqn. (5) to a measured impedance spectrum will result in arbitrary sets of ζ and χ_1 whose product meets the experimental data and therefore no reliable information about ohmic and charge transfer losses in the electrode will be accessible. To enable a meaningful analysis it is essential to measure at least one of those parameters independently. This approach was realized in [58] and [60], the impedance of a nickel / yttria doped zirconia (YSZ) cermet anode was investigated by means of impedance spectroscopy and corresponding impedance simulations. For these simulations all model parameters were calculated based on (i) conductivity data measured on bulk samples of respective materials, (ii) the line specific charge transfer resistance of the three phase boundary as well as related charge transfer and interfacial capacities evaluated by means of patterned model anodes [61] and (iii) microstructural information as volume fractions and tortu-

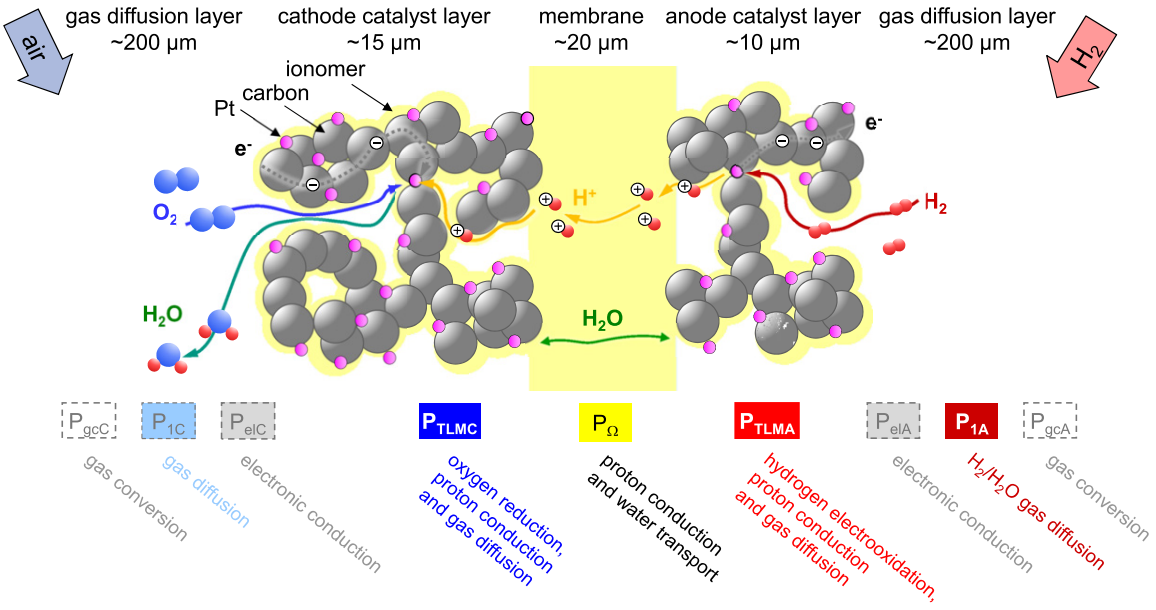

Figure 6: Polarization processes in the porous electrodes of a PEMFC. Transport and electrochemical reactions in the cathode catalyst layer (CCL) and the anode catalyst layer (ACL) can be described by TLMs considering the coupling of proton conduction in the ionomer, electrochemical reactions at the noble metal catalyst, electronic transport in the carbon support and gas diffusion in the pores. To avoid unused platinum catalyst the thickness of the electrochemically active regions should meet the thickness of CCL and ACL respectively. The gas diffusion layers (GDL) enable a homogeneous current collection and gas supply.

osities obtained by FIB-SEM tomography [62]. It could be shown that impedance simulations based on reliable material and microstructural parameters can provide spectra close to measured ones without fitting of any parameter. Under some conditions as a rather dense and thick anode layer a 3 channel TLM (Fig. 1 (f)) is required that additionally considers the gas diffusion in the electrochemically active layer [60].

3.2 Polymer electrolyte membrane fuel cells

In case of PEMFCs the microstructural analysis of porous electrodes is by far more challenging as microstructural features extend over several orders of magnitude (nanoscaled catalysts to several 10 µm thick electrodes), the materials are compressible and their volume is affected by water uptake. Furthermore liquid water in the pores affects the transport properties. The same holds for the measurement of reliable electrochemical parameters of the applied electrocatalysts by means of model systems [63].

Thus the TLM modeling of PEMFC electrodes relies on impedance measurements performed under appropriate conditions. A significant advantage in a PEMFC is that the overall anode polarization resistance can be minimized down to $\sim 10\,\mathrm{m\Omega{\cdot}cm^2}$ by applying appropriate fuel compositions and the impedance spectrum is dominated by two processes at the cathode – gas diffusion in the GDL and oxygen reduction [64]. The oxygen reduction can be described by a TLM considering the electrochemical oxygen reduction reaction (ORR) at the noble metal catalyst and its coupling with the protonic transport in the ionomer (see Fig. 1 (e)). The electronic transport can be neglected. The same holds true for the gas diffusion in the CCL, for low current densities and no flooding of pores it can be neglected in the CNLS-fit.

An appropriate parameterization of the TLM becomes possible as characteristic operating parameter dependencies of the TLM-parameters ionomer ($r_{ion} = r_s$) and charge transfer resistance ($r_{ct} = r_p$) can be used. In [59] it is shown that the resistance of the ionomer r_{ion} is significantly affected by the relative humidity RH of the supplied gas whereas the current density has only a minor impact that is limited to high current densities. On the other hand the charge transfer resistance r_{ct} showed a strong dependency on the current but is not significantly influenced by the humidity. Furthermore the rather small CCL thickness enables operating conditions that extend the penetration depth where the impact of the proton transport in the ionomer can be neglected and the CCL is homogenously utilized ($\lambda \gg L$), providing direct access to the charge transfer resistance.

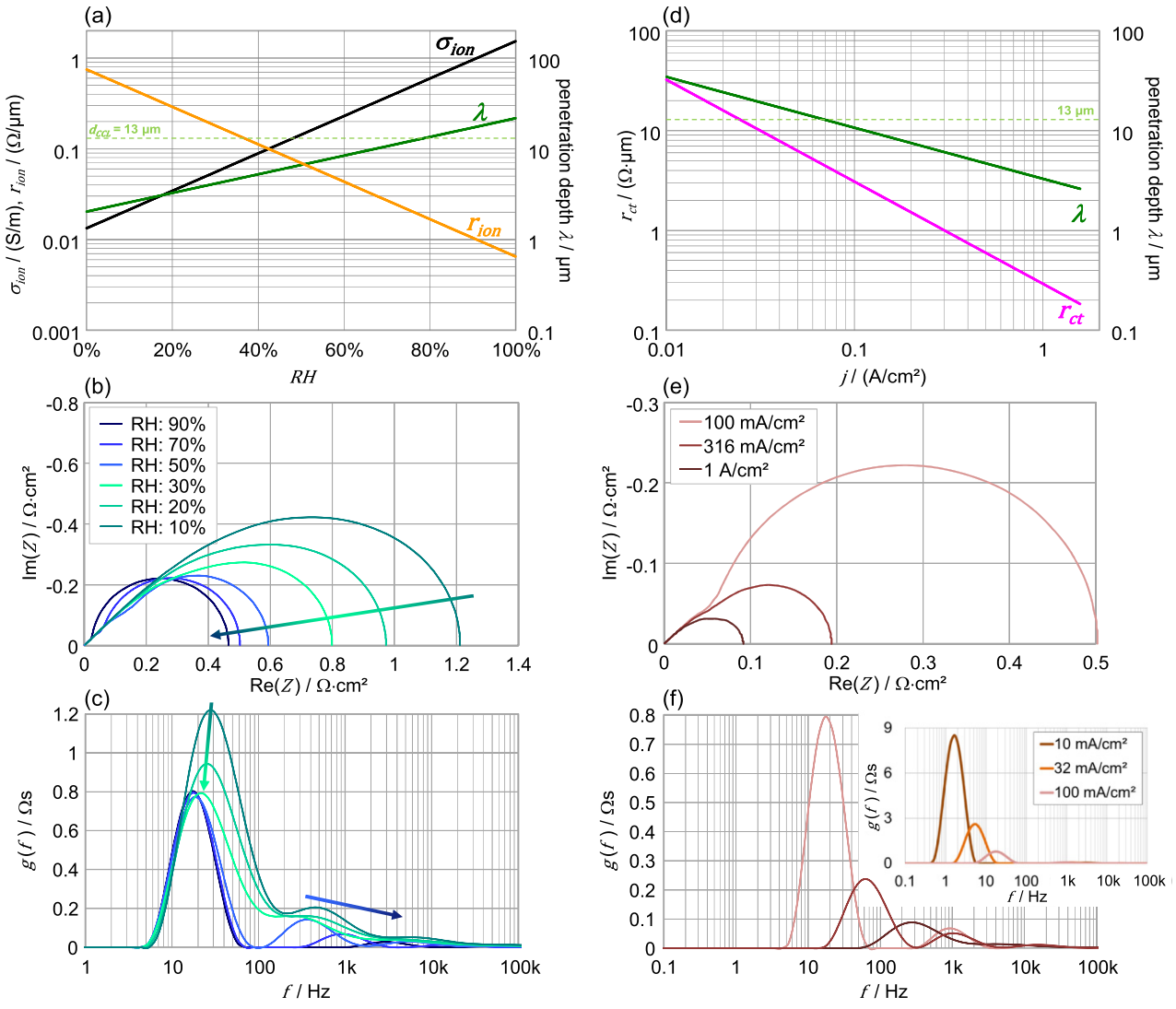

Figure 7: Impact of relative humidity and current density on the TLM-impedance of the cathode catalyst layer in a PEMFC. The data is calculated for a temperature of 80 °C and a fixed current density of 100 mA/cm² (a–c) and relative humidity of 70 % (d–f) applying the parameters published in [59].

In Fig. 7 impedance spectra, the related DRTs and the TLM-parameters calculated according to the dependencies observed in [59] are displayed for a variation of *RH* and current density. To illustrate the dependencies, a TLM equivalent circuit according to Fig. 1 (e) with a constant c_p-value is applied and the gas diffusion impedance is excluded. With increasing relative humidity the ionomer conductivity increases. This is resulting in a significant reduction of the related transport resistance r_{ion} and an increase of the penetration depth (Fig. 7 (a)). With diminishing impact of the transport resistance the whole electrode thickness is more and more homogenously used. The shape of the spectrum changes from the characteristic TLM impedance to the semicircle of an RC element (Fig. 7 (b)). In the DRT the main peak at 20 to 30 Hz representing the oxygen reduction at the Pt-catalyst decreases down to a certain point (here at RH ~ 50 %) were a sufficient proton transport in the ionomer is achieved and the platinum catalyst is homogenously used over the entire electrode thickness. A further increase in RH will have no more influence on this peak, only the side peaks at higher relaxation frequencies, representing the proton transport through the electrode, are reduced and shifted towards higher relaxation frequencies (Fig. 7 (c)).

The current density shows an even stronger impact on the polarization resistance as r_{ct} is decreasing significantly with increasing current density. As a result the penetration depth is decreasing too. This is related to the charge

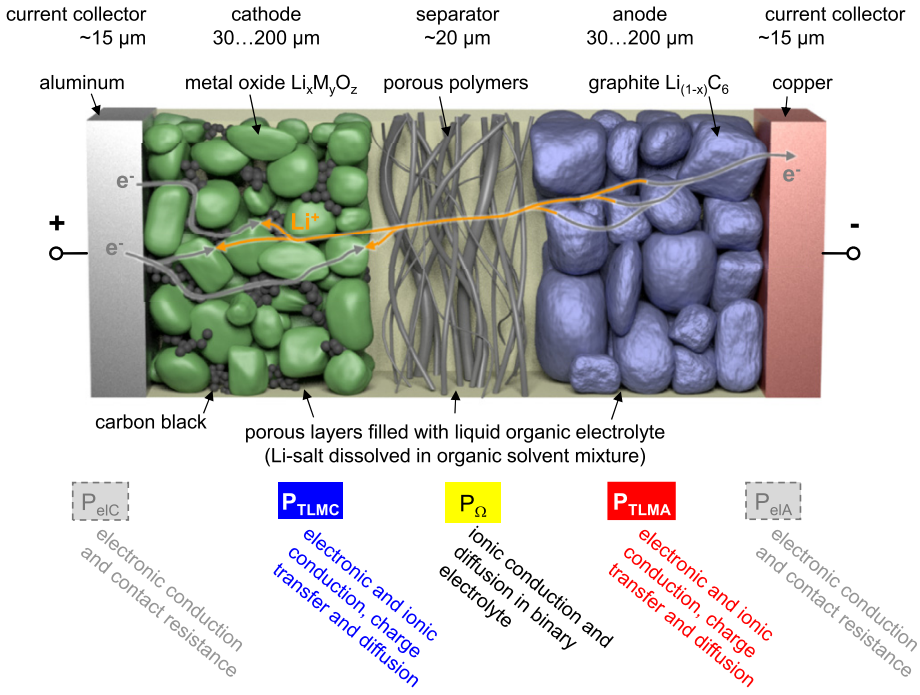

Figure 8: Sketch of a lithium ion battery exhibiting two porous intercalation electrodes coated onto the current collectors. The ionic transport in the electrolyte is significantly affected by the microstructure (porosity and tortuosity) of separator and electrodes. For a sufficient electronic conductivity in the cathode a carbon black / binder phase connecting the active material particles is mandatory.

transfer current density distribution in the CCL. Due to a limited proton transport in the ionomer, at high current densities a major part of the charge transfer takes place close to the membrane, the penetration depth is below the CCL thickness and the characteristic TLM impedance is observed (Fig. 7 (d, e)). Concerning the catalyst utilization under these conditions a certain part of the catalyst far away from the membrane is used to a lesser extent. At low current densities in the range of a few 10 mA/cm² the high r_{ct}-value is the limiting factor whereas the proton transport is sufficiently fast, resulting in RC-type impedance and a single peak at the related relaxation frequency in the DRT (Fig. 7 (f)). In the plots shown here the relaxation frequencies are only determined by the r_{ct}-value, any current density or RH dependency of the double layer and charge transfer capacity, as well as capacitive effects along the transport path, is neglected. Furthermore it has to be stated that the current density dependency of r_{ct} will lead to a variation of this value over the CCL thickness, which will increase with the current density. Such variations are not considered in the TLM impedance according to eqn. (1) and eqn. (5) respectively. To consider any kind of material or microstructural variation over the electrode thickness more advanced numerical TLM calculation approaches as presented in [60] can be applied.

3.3 Lithium ion batteries

Fig. 8 displays the layer structure of a lithium ion battery exhibiting particulate electrode layers that are coated onto thin metal foil current collectors. Electronic and ionic transport in the porous cathode and anode are coupled via the charge transfer reactions at the particle surfaces. Considering the coupling of those processes one TLM per electrode is required to model the cell's impedance.

In TLMs for lithium ion battery electrodes a much more complex shunt branch impedance ζ is required, considering at least charge transfer reaction at the liquid electrolyte / active material interface and Li-diffusion in the active material. Furthermore resistive layers on particle surfaces, as the solid electrolyte interface (SEI), as well as diffusive processes in the electrolyte volume close to the active material are of relevance. In case of a low electronic conductivity of the electrode $\chi_2 = r_{electron}$ has to be considered in addition to the ionic conductivity $\chi_1 = r_{ion}$. Furthermore diffusive processes in the binary electrolyte, exhibiting mobile cations and anions, affect the impedance of a lithium ion battery electrode. Thus rather complex ECMs as displayed in Fig. 8 have to be applied. One should notice that this ECM contains a TLM describing the Li-diffusion in the active material within a TLM representing the overall electrode.

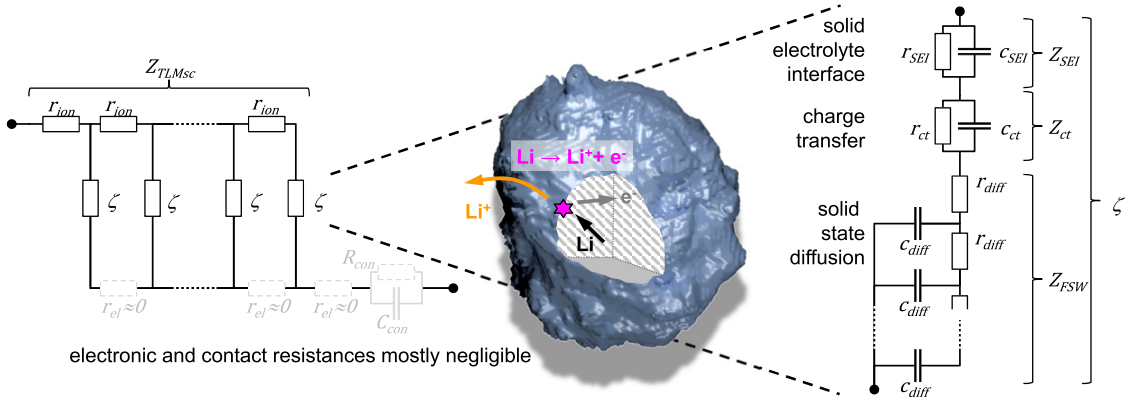

Figure 9: Transmission line impedance of a graphite anode in lithium ion batteries. Due to the high electronic conductivity of graphite ($r_{ion} \gg r_{el}$), electronic resistance r_{el} and contact resistance R_{con} are often negligible. The shunt branch impedance ζ represents the processes at the active material / liquid electrolyte interface (SEI and charge transfer impedance: Z_{SEI}, Z_{ct}) and the Li-diffusion inside the particles described by a finite space Warburg impedance Z_{FSW}. The image in the center displays one graphite particle extracted from a µCT-reconstruction of a graphite anode. Diffusive processes in the electrolyte are not considered in this TLM.

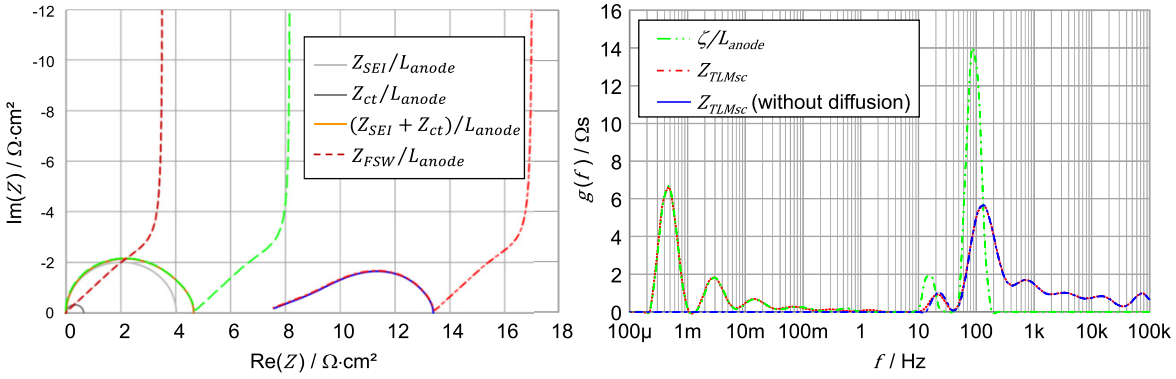

Figure 10: Impedance spectra and DRTs of the equivalent circuit and its elements as displayed in Fig. 9. The parameterization is based on the values given in Table 1 and further parameters listed in the text above.

The spectra and related DRT's of the different elements are displayed in Fig. 10. The parameters for the different equivalent circuit elements in the TLM are taken from Table 1 (high power cell), the Li-diffusion in the active material is described by a finite space Warburg element according to eqn. (6) with $\tau_{diff} = r_{graphite}^2/D_{Li}$ (average graphite particle radius: $r_{graphite} = 6\,\mu m$, lithium diffusion coefficient in graphite: $D_{Li} = 10^{-10}\,cm^2/s$ [65]) and $r_{diff} \cdot L = r_{graphite}/(C_0 \cdot D_{Li})$ (volume specific capacity: $C_0 = 29\,kF/cm^3$). In the DRT the rather slow Li-diffusion in the active material is clearly separated from the interfacial processes at the graphite / liquid electrolyte interface. Furthermore the low frequency part of the spectrum is barely influenced by the ionic transport of lithium in the pores. At higher frequencies clear differences between the shunt branch impedance only (ζ/L_{anode}, which equals Z_{TLMsc} for $r_{ion} = 0$) and the TLM impedance Z_{TLMsc} are obvious in the spectrum and the DRT. Due to the limited ionic conductivity in the pores of the electrode, the two processes, which are represented by a resistance and a parallel capacitance each, are expanded towards higher frequencies. It should be noted that the total polarization resistance of the TLM impedance Z_{TLMsc} is exceeding the polarization resistance of the overall shunt branch impedance ζ/L_{anode}. Despite of the DRT peak height ratio at ~ 20 and ~ 100 Hz, the total area underneath the DRT-curve of Z_{TLMsc} is exceeding that of ζ/L_{anode}.

The comparison of the TLM impedance Z_{TLMsc} and its DRT with and without consideration of the lithium diffusion shows no differences for frequencies above 1 Hz. Due to the different time constants a simplification of the TLM can be performed to focus on certain processes, e. g. parts of the shunt branch with low relaxation frequencies as the Li-diffusion can be neglected. With this ap-

Table 1: Microstructural, electrical and electrochemical parameters of two different graphite anodes.

cell type	high power cell	high energy cell
cell ID (manufacturer: Kokam)	SLB283452	SLPB353452
anode thickness L_{anode}	55 µm	90 µm
graphite volume fraction $\varepsilon_{graphite}$	65.8 %	75.2 %
pore volume fraction ε_{pore}	34.2 %	24.8 %
tortuosity of pore phase τ_{pore}	2.5	5.1
volume specific graphite surface $a_{graphite}$	0.35 $cm^2 m^{-1}$	0.31 μm^{-1}
effective ionic conductivity σ_{ion}	0.108 S/m	0.039 S/m
TLM charge transfer resistance r_{ct} (CNLS-fit)	0.64 $\Omega \cdot cm^2$	0.43 $\Omega \cdot cm^2$
TLM SEI resistance r_{SEI} (CNLS-fit)	4.02 $\Omega \cdot cm^2$	2.75 $\Omega \cdot cm^2$
graphite surface area specific charge transfer resistance $r_{ct,graphite}$	12.3 $\Omega \cdot cm^2$	12.2 $\Omega \cdot cm^2$
graphite surface area specific SEI resistance $r_{SEI,graphite}$	77.4 $\Omega \cdot cm^2$	77.7 $\Omega \cdot cm^2$
exchange current density at graphite / liquid electrolyte interface i_0	2.1 mA/cm²	2.1 mA/cm²

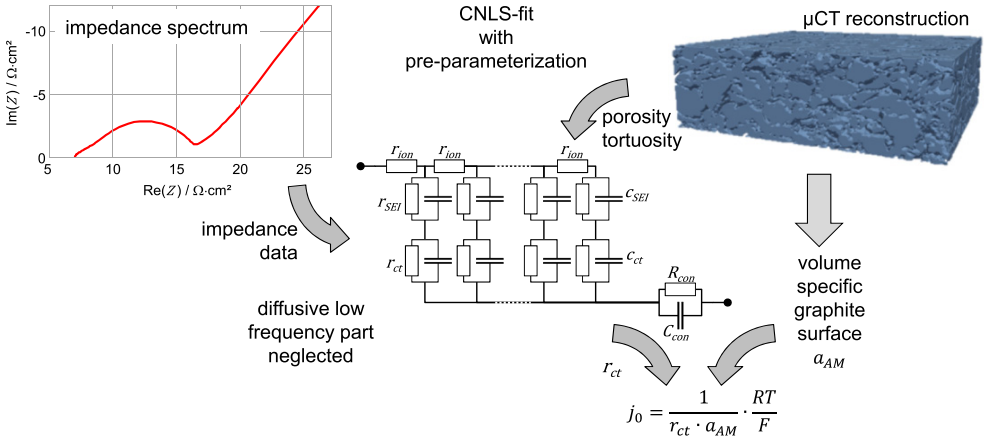

Figure 11: Quantification of the exchange current density by means of a pre-parameterized TLM-fit. The effective ionic conductivity r_{ion} in the porous electrode is calculated based on microstructural parameters and the electrolyte's bulk conductivity and further on fixed in CNLS-fit of the TLM to the measured spectra. The exchange current density j_0 of the graphite / liquid electrolyte interface is calculated by relating the charge transfer resistance to the volume specific graphite surface area obtained from the microstructure reconstruction.

proach essential material and interfacial parameters become accessible by combining electrochemical and microstructural data in the TLM. One important parameter is the exchange current density i_0 at the active material / liquid electrolyte interface, which is required to model the nonlinear current/overvoltage relation of the charge transfer process.

To quantify the exchange current density processes within a porous electrode a pre-parameterization during the CNLS-fit of the TLM is required to eliminate the ambiguity previously discussed. The procedure [66] is sketched in Fig. 11.

The effective ionic conductivity calculated by eqn. (2) using porosity and tortuosity values from the reconstruction is kept as a fixed value in the CNLS-fit of the TLM. Furthermore, the impact of the low frequency diffusion processes and the capacitive branch are minimized by neglecting impedance data below 100 mHz in the CNLS fit. Based on this approach the graphite anodes of two commercial pouch cells were compared by (i) a µCT-analysis and subsequent microstructure reconstruction and parameter evaluation as described in [27] and a subsequent CNLS-fitting of the spectra using the microstructural data for pre-parameterization. The evaluated parameters are summarized in Table 1, CNLS-fit results are displayed in Fig. 12.

Whereas clear differences with respect to layer thickness, microstructure and CNLS-fitting results are obvious, the parameters reflecting the graphite / liquid electrolyte interface ($r_{ct,graphite}$, $r_{SEI,graphite}$, i_0) are identical for both electrodes. This result shows that the TLM approach can provide reliable information about electrochemical systems if the microstructural features of the porous electrode are appropriately considered.

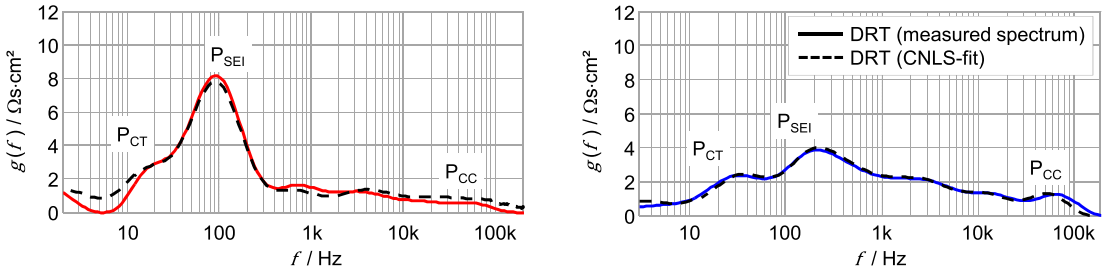

Figure 12: DRTs of the spectra of the two cells listed in Table 1. A good agreement between the DRTs of the measured and the spectrum simulated using the fitting result is achieved for both cells.

4 Summary

In this paper examples for the application of impedance spectroscopy for the analysis of technical electrodes in batteries and fuel cells are presented. It is shown that the inherent coupling of transport processes and electrochemical reactions in porous, multiphase electrodes requires complex transmission line models for a physicochemical meaningful impedance modeling. The distribution of relaxation times is an indispensable tool for the deconvolution of impedance spectra and the separation of overlapping electrode processes. In case of a transmission line impedance the existence of multiple peaks in the DRT is an error source that impedes the analysis. The resulting DRT is strongly affected by (i) the impedance data quality and resolution as well as (ii) the selected regularization parameter for the numerical DRT calculation. A proper deconvolution becomes impossible for strongly overlapping TLMs within an impedance spectrum. Other measures as varied operating conditions, which affect individual polarization phenomena and their time constants, are required.

The application of a DRT-based transmission line modeling is discussed for three types of electrochemical cells, namely solid oxide cells, polymer electrolyte membrane fuel cells and lithium ion batteries. It is shown that TLM-modeling relying on impedance data only is prone to error. In many cases additional information about microstructural features and effective transport in the investigated electrode are essential for a physicochemically meaningful model and a correct parameterization. Depending on the type of cell, different approaches were proven to be feasible as (i) the evaluation of electrode parameters from model systems, (ii) the use of operating parameter variations to selectively modify transport processes and (iii) the application of microstructural parameter obtained by tomography. Based on such approaches fundamental information about the processes in the electrode become accessible, reliable models can be designed and material and interfacial parameters can be quantified.

Funding: The financial support of the Deutsche Forschungsgemeinschaft throughout the project 281041241/GRK2218 “SiMET”, the Bundesministerium für Bildung und Forschung BMBF throughout the project 03SF0494F “SOFC Degradation”, the Bundesministerium für Wirtschaft und Energie BMWi throughout the projects 03ET6101B “KerSOLife100” and 03ETB005E “KOSOS”, the Schaeffler Technologies AG & Co. KG throughout the PhD-project “Modelling of PEM Fuel Cells” and the Friedrich und Elisabeth Boysen-Stiftung throughout the project BOY121 “Determination of charge transfer parameters in lithium ion batteries” is gratefully acknowledged.

References

1. W. R. Grove, LXXII. On a gaseous voltaic battery, The London, Edinburgh and Dublin Philosophical Magazine and Journal of Science 21, pp. 417–420 (1842).
2. J. R. Macdonald, Impedance Spectroscopy, New York: John Wiley & Sons (1987).
3. E. Barsoukov, J. R. Macdonald, Impedance Spectroscopy: Theory, Experiment, and Applications, Hoboken NJ: Wiley-Interscience (2005).
4. M. E. Orazem, B. Tribollet, Electrochemical Impedance Spectroscopy, Hoboken, NJ: John Wiley & Sons, Inc. (2008).
5. A. Lasia, Electrochemical Impedance Spectroscopy and its Applications, London: Springer (2014).
6. D. Klotz, A. Weber, E. Ivers-Tiffée, Practical guidelines for reliable electrochemical characterization of solid oxide fuel cells, Electrochim Acta 227, pp. 110–126 (2017).
7. B. A. Boukamp, A linear Kronig–Kramers Transform test for immittance data validation, J. Electrochem. Soc. 142, pp. 1885–1894 (1995).
8. M. Schönleber, D. Klotz, E. Ivers-Tiffée, A method for improving the robustness of linear Kramers-Kronig validity tests, Electrochim Acta 131, pp. 20–27 (2014).
9. M. Schönleber, http://www.iam.kit.edu/wet/english/Lin-KK.php (2015).
10. H. Schichlein, A. C. Müller, M. Voigts, A. Krügel, E. Ivers-Tiffée, Deconvolution of electrochemical impedance spectra for the identification of electrode reaction mechanisms in solid oxide

fuel cells, Journal of Applied Electrochemistry 32, pp. 875–882 (2002).
11. E. Ivers-Tiffée, A. Weber, Evaluation of electrochemical impedance spectra by the distribution of relaxation times, Journal of the Ceramic Society of Japan 125, pp. 193–201 (2017).
12. S. Dierickx, A. Weber, E. Ivers-Tiffée, How the distribution of relaxation times enhances complex equivalent circuit models for fuel cells, Electrochim Acta 355, 136764 (2020).
13. A. Leonide, V. Sonn, A. Weber, E. Ivers-Tiffée, Evaluation and modeling of the cell resistance in anode-supported solid oxide fuel cells, J. Electrochem. Soc. 155, pp. B36–B41 (2008).
14. J. P. Schmidt et al., Studies on $LiFePO_4$ as cathode material using impedance spectroscopy, J. Power Sources 196, pp. 5342–5348 (2011).
15. J. Euler, W. Nonnenmacher, Stromverteilung in porösen Elektroden, Electrochim Acta 2, pp. 268–286 (1960).
16. J. S. Newman, C. W. Tobias, Theoretical analysis of current distribution in porous electrodes, J. Electrochem. Soc. 109, pp. 1183–1191 (1962).
17. K. J. Euler, Die Verteilung der Stromdichte über die Dicke von ebenen porösen Gas-Elektroden in elektrochemischen Stromquellen, Ann. Phys. 481, pp. 257–266 (1971).
18. M. Doyle, T. F. Fuller, J. Newman, Modeling of galvanostatic charge and discharge of the lithium/polymer/insertion cell, J. Electrochem. Soc. 140, pp. 1526–1533 (1993).
19. T. F. Fuller, M. Doyle, J. Newman, Simulation and optimization of the dual lithium ion insertion cell, J. Electrochem. Soc. 141, pp. 1–10 (1994).
20. R. M. Darling, J. Newman, Modeling a porous intercalation electrode with two characteristic particle sizes, J. Electrochem. Soc. 144, pp. 4201–4208 (1997).
21. M. Ender, An extended homogenized porous electrode model for lithium-ion cell electrodes, J. Power Sources 282, pp. 572–580 (2015).
22. W. G. Bessler, S. Gewies, M. Vogler, A new framework for physically based modeling of solid oxide fuel cells, Electrochim Acta 53, pp. 1782–1800 (2007).
23. W. G. Bessler et al., Model anodes and anode models for understanding the mechanism of hydrogen oxidation in solid oxide fuel cells, Phys. Chem. Chem. Phys. 12, pp. 13888–13903 (2010).
24. J. R. Wilson et al., Three-dimensional reconstruction of a solid-oxide fuel-cell anode, Nature Materials 5, pp. 541–544 (2006).
25. M. Ender, J. Joos, T. Carraro, E. Ivers-Tiffée, Three-dimensional reconstruction of a composite cathode for lithium-ion cells, Electrochemistry Communications 13, pp. 166–168 (2011).
26. J. R. Izzo et al., Nondestructive reconstruction and analysis of SOFC anodes using x-ray computed tomography at sub-50 nm resolution, J. Electrochem. Soc. 155, pp. B504–B508 (2008).
27. M. Ender, J. Joos, A. Weber, E. Ivers-Tiffée, Anode microstructures from high-energy and high-power lithium-ion cylindrical cells obtained by X-ray nano-tomography, J. Power Sources 269, pp. 912–919 (2014).
28. B. Rüger, A. Weber, E. Ivers-Tiffée, 3D-modelling and performance evaluation of mixed conducting (MIEC) cathodes, ECS Trans. 7, pp. 2065–2074 (2007).
29. B. Rüger, J. Joos, T. Carraro, A. Weber, E. Ivers-Tiffée, 3D electrode microstructure reconstruction and modelling, ECS Trans. 25, pp. 1211–1220 (2009).
30. P. R. Shearing et al., Microstructural analysis of a solid oxide fuel cell anode using focused ion beam techniques coupled with electrochemical simulation, J. Power Sources 195, pp. 4804–4810 (2010).
31. M. Doyle, J. P. Meyers, J. Newman, Computer simulations of the impedance response of lithium rechargeable batteries, J. Electrochem. Soc. 147, pp. 99–110 (2000).
32. J. P. Meyers, M. Doyle, R. M. Darling, J. Newman, The impedance response of a porous electrode composed of intercalation particles, J. Electrochem. Soc. 147, pp. 2930–2940 (2000).
33. W. G. Bessler, A new computational approach for SOFC impedance from detailed electrochemical reaction-diffusion models, Solid State Ionics 176, pp. 997–1011 (2005).
34. A. Häffelin, J. Joos, M. Ender, A. Weber, E. Ivers-Tiffée, Time-dependent 3D impedance model of mixed-conducting solid oxide fuel cell cathodes, J. Electrochem. Soc. 160, pp. F867–F876 (2013).
35. B. A. Boukamp, A nonlinear least squares fit procedure for analysis of immittance data of electrochemical systems, Solid State Ionics 20, pp. 31–44 (1986).
36. B. A. Boukamp, A package for impedance/admittance data analysis, Solid State Ionics 18-19, pp. 136–140 (1986).
37. J. R. Macdonald, Comparison and application of two methods for the least squares analysis of immittance data, Solid State Ionics 58, pp. 97–107 (1992).
38. A. Jossen, Fundamentals of battery dynamics, J. Power Sources 154, pp. 530–538 (2006).
39. D. Andre et al., Characterization of high-power lithium-ion batteries by electrochemical impedance spectroscopy. I. Experimental investigation, J. Power Sources 196, pp. 5334–5341 (2011).
40. D. Andre et al., Characterization of high-power lithium-ion batteries by electrochemical impedance spectroscopy. II: Modelling, J. Power Sources 196, pp. 5349–5356 (2011).
41. J. P. Schmidt, P. Berg, M. Schönleber, A. Weber, E. Ivers-Tiffée, The distribution of relaxation times as basis for generalized time-domain models for Li-ion batteries, J. Power Sources 221, pp. 70–77 (2013).
42. G. J. Brug, A. L. G. van den Eeden, J. H. Sluyters, The analysis of electrode impedance complicated by the presence of a constant phase element, J. Electroanal. Chem. 176, pp. 275–295 (1984).
43. A. Bieberle, L. J. Gauckler, Reaction mechanism of Ni pattern anodes for solid oxide fuel cells, Solid State Ionics 135 pp. 337–345 (2000).
44. R. Barfod et al., Detailed characterization of anode-supported SOFCs by impedance spectroscopy, J. Electrochem. Soc. 154, pp. B371–B378 (2007).
45. E. Warburg, Über das Verhalten sogenannter unpolarisirbarer Elektroden gegen Wechselstrom, Ann. Phys. 303, pp. 493–499 (1899).
46. J. C. Wang, Realizations of generalized Warburg impedance with RC ladder networks and transmission lines, J. Electrochem. Soc. 134, pp. 1915–1920 (1987).
47. H. Gerischer, Wechselstrompolarisation von Elektroden mit einem potentialbestimmenden Schritt beim Gleichgewichtspotential I, Zeitschrift für Physikalische Chemie 198, pp. 286–313 (1951).
48. N. Wagner, Application of impedance spectroscopy in fuel cell research, TM - Technisches Messen 78, pp. 30–35 (2011).

49. B. A. Boukamp, H. J. M. Bouwmeester, Interpretation of the Gerischer impedance in solid state ionics, Solid State Ionics 157, pp. 29–33 (2003).
50. S. B. Adler, J. A. Lane, B. C. H. Steele, Electrode kinetics of porous mixed-conducting oxygen electrodes, J. Electrochem. Soc. 143, pp. 3554–3564 (1996).
51. C. Endler-Schuck, J. Joos, C. Niedrig, A. Weber, E. Ivers-Tiffée, The chemical oxygen surface exchange and bulk diffusion coefficient determined by impedance spectroscopy of porous $La_{0.58}Sr_{0.4}Co_{0.2}Fe_{0.8}O_3$-$\delta$ (LSCF) cathodes, Solid State Ionics 269, pp. 67–79 (2015).
52. J. Weese, A reliable and fast method for the solution of Fredholm integral equations of the first kind based on Tikhonov regularization, Computer Physics Communications 69, pp. 99–111 (1992).
53. A. Kromp, H. Geisler, A. Weber, E. Ivers-Tiffée, Electrochemical impedance modeling of gas transport and reforming kinetics in reformate fueled solid oxide fuel cell anodes, Electrochim Acta 106, pp. 418–424 (2013).
54. C. Endler-Schuck et al., Performance analysis of mixed ionic-electronic conducting cathodes in anode supported cells, J. Power Sources 196, pp. 7257–7262 (2011).
55. N. Russner, S. Dierickx, A. Weber, R. Reimert, E. Ivers-Tiffée, Multiphysical modelling of planar solid oxide fuel cell stack layers, J. Power Sources 451, 227552 (2020).
56. A. Leonide, B. Rüger, A. Weber, W. A. Meulenberg, E. Ivers-Tiffée, Impedance study of alternative (La,Sr)FeO_3-δ and (La,Sr)(Co,Fe)O_3-δ MIEC cathode compositions, J. Electrochem. Soc. 157, pp. B234–B239 (2010).
57. L. Almar, J. Szasz, A. Weber, E. Ivers-Tiffée, Oxygen transport kinetics of mixed ionic-electronic conductors by coupling focused ion beam tomography and electrochemical impedance spectroscopy, J. Electrochem. Soc. 164, pp. F289–F297 (2017).
58. S. Dierickx, J. Joos, A. Weber, E. Ivers-Tiffée, Advanced impedance modelling of Ni/8YSZ cermet anodes, Electrochim Acta 265, pp. 736–750 (2018).
59. M. Heinzmann, A. Weber, E. Ivers-Tiffée, Impedance modelling of porous electrode structures in polymer electrolyte membrane fuel cells, J. Power Sources 444, 227279 (2019).
60. S. Dierickx, T. Mundloch, A. Weber, E. Ivers-Tiffée, Advanced impedance model for double-layered solid oxide fuel cell cermet anodes, J. Power Sources 415, pp. 69–82 (2019).
61. A. Utz, H. Störmer, A. Leonide, A. Weber, E. Ivers-Tiffée, Degradation and relaxation effects of Ni patterned anodes in H_2/H_2O atmosphere, J. Electrochem. Soc. 157, pp. B920–B930 (2010).
62. J. Joos, M. Ender, I. Rotscholl, N. Menzler, E. Ivers-Tiffée, Quantification of double-layer Ni/YSZ fuel cell anodes from focused ion beam tomography data, J. Power Sources 246, pp. 819–830 (2014).
63. S. Martens et al., A comparison of rotating disc electrode, floating electrode technique and membrane electrode assembly measurements for catalyst testing, J. Power Sources 392, pp. 274–284 (2018).
64. M. Heinzmann, A. Weber, E. Ivers-Tiffée, Advanced impedance study of polymer electrolyte membrane single cells by means of distribution of relaxation times, J. Power Sources 402, pp. 24–33 (2018).
65. M. D. Levi, D. Aurbach, Diffusion coefficients of lithium ions during intercalation into graphite derived from the simultaneous measurements and modeling of electrochemical impedance and potentiostatic intermittent titration characteristics of thin graphite electrodes, Journal of Physical Chemistry B 101, pp. 4641–4647 (1997).
66. J. Costard, Einfluss von Mikrostruktur und Materialparametern auf die Leistungsfähigkeit poröser Elektroden für Lithium-Ionen Batterien, Dissertation Karlsruher Institut für Technologie (KIT) (2018).

Bionotes

André Weber
Karlsruhe Institute of Technology (KIT),
Institute of Applied Materials (IAM-WET),
Adenauerring 20b, 76131 Karlsruhe,
Germany
andre.weber@kit.edu

André Weber is working as senior scientist (Akademischer Oberrat) at the Institute for Applied Materials (IAM-WET) at Karlsruhe Institute of Technology (KIT), Germany. Actually he is heading two groups related to fuel cells and & electrolyzer and battery research. His research is related to the electrical testing and modeling of fuel cells, electrolyzers and batteries, with a special emphasis on the detailed electrochemical characterization by means of impedance spectroscopy. The experimental and theoretical work of his research groups ranges from fundamental studies on model systems to the analysis of commercial products, aiming at a model based understanding of the complex coupling of electrochemical reactions and transport mechanisms within electrochemical devices. He has co-authored several book chapters, and more than 100 peer-reviewed journal papers on scientific topics related to fuel cells and batteries (https://scholar.google.de/citations?hl=de&user=IGECnVQAAAAJ). Web: http://www.iam.kit.edu/wet/english/mitarbeiter_andre_weber.php.